# Fabrication and Characterization of Electrospun Chitosan Nanofibers Formed via Templating with Polyethylene Oxide

Satyajeet S. Ojha,[†] Derrick R. Stevens,[‡] Torissa J. Hoffman,[‡] Kelly Stano,[†] Rebecca Klossner,[§] Mary C. Scott,[‡] Wendy Krause,[†,§] Laura I. Clarke,[‡] and Russell E. Gorga*[,†,§]

*Department of Textile Engineering, Chemistry and Science, Department of Physics, and Fiber and Polymer Science Program, North Carolina State University, Raleigh, North Carolina 27695*

*Received May 20, 2008; Revised Manuscript Received July 16, 2008*

Chitosan is an abundantly common, naturally occurring, polysaccharide biopolymer. Its biocompatible, biodegradable, and antimicrobial properties have led to significant research toward biological applications such as drug delivery, artificial tissue scaffolds for functional tissue engineering, and wound-healing dressings. For applications such as tissue scaffolding, formation of highly porous mats of nanometer-sized fibers, such as those fabricated via electrospinning, may be quite important. Previously, strong acidic solvents and blending with synthetic polymers have been used to achieve electrospun nanofibers containing chitosan. As an alternative approach, in this work, polyethylene oxide (PEO) has been used as a template to fabricate chitosan nanofibers by electrospinning in a core-sheath geometry, with the PEO sheath serving as a template for the chitosan core. Solutions of 3 wt % chitosan (in acetic acid) and 4 wt % PEO (in water) were found to have matching rheological properties that enabled efficient core-sheath fiber formation. After removing the PEO sheath by washing with deionized water, chitosan nanofibers were obtained. Electron microscopy confirmed nanofibers of ~250 nm diameter with a clear core-sheath geometry before sheath removal, and chitosan nanofibers of ~100 nm diameter after washing. The resultant fibers were characterized with IR spectroscopy and X-ray diffraction, and the mechanical and electrical properties were evaluated.

## Introduction

Electrospinning is a technique used to generate fibers at the submicron scale, yielding a three-dimensional porous network (a random mat) of nanofibers with high aspect ratio and a large specific surface area.[1−6] A typical electrospinning apparatus includes a polymer solution or melt in a syringe, charged through a high voltage supply, and a grounded plate placed at a fixed distance from the needle tip. Due to the large potential difference, the surface tension of the fluid droplet at the tip of the metal syringe needle is overcome and a Taylor cone is formed, whereby a fluid jet is ejected and subjected to whipping instabilities due to electric Maxwell stresses.[7] In addition, the rheological properties of the polymer solution are important; in particular, to form fibers, a solution must have a sufficient concentration such that the polymer chains are entangled and a suitable viscosity at this concentration so a droplet can be maintained and the solution can be pumped through the syringe. Shenoy et al.[8] was able to determine the role of chain entanglements on fiber formation for electrospinning by characterizing the number of entanglements per chain ($n_e$). For a polymer solution,

$$(n_e)_{soln} = (\phi_p \times M_w)/(M_e)_{soln} \quad (1)$$

where $M_w$ is the molecular weight of the polymer, $M_e$ is the entanglement molecular weight, and $\varphi_p$ is the volume fraction or concentration of polymer. The number of chain entanglements per chain must be equal to or greater than 3.5 for complete stable fiber formation.

Recently several groups have fabricated electrospun nanofibers having a core-sheath geometry.[9−15] In our approach (Figure 1), two concentric needles are arranged in an annular fashion, and the two different polymer solutions form a compound pendant drop at the capillary end, resulting in a compound Taylor cone. Mixing between the two components is limited because the evaporation of the solvent is very rapid.[16] For fabrication of core-sheath nanofibers (without a hollow tube structure), it is essential that both core and sheath fluid are sufficiently viscous and the solvents are immiscible,[15] thus, the rheological properties of the two solutions must be well matched.[16] Therefore, the zero shear viscosity of the polymer solution is a good metric to determine the compatibility of potential solutions for bicomponent electrospinning.

Here we demonstrate that coaxial electrospinning is a powerful approach in cases where a particular polymer solution/melt is not capable of forming nanofibers due to its fluid characteristics such as poor solubility and a viscosity window that does not generate a critical entanglement density for fiber formation.[17] For instance, the critical entanglement density for the important biomaterial chitosan cannot be easily reached without gel formation.[18] As shown below, by using coaxial electrospinning, a chitosan solution does not have to meet the entanglement threshold for fiber formation to occur but merely match the zero shear flow viscosity of the template polymer solution (here PEO), where the template polymer solution is above its critical entanglement density. Moreover, as many potential templates (polymers with known electrospinning characteristics) are available, we believe this technique will be powerful in expanding electrospinning to previously inaccessible

* To whom correspondence should be addressed. E-mail: regorga@ncsu.edu.
[†] Department of Textile Engineering, Chemistry and Science.
[‡] Department of Physics.
[§] Fiber and Polymer Science Program.

10.1021/bm800551q CCC: $40.75 
Published on Web 08/15/2008

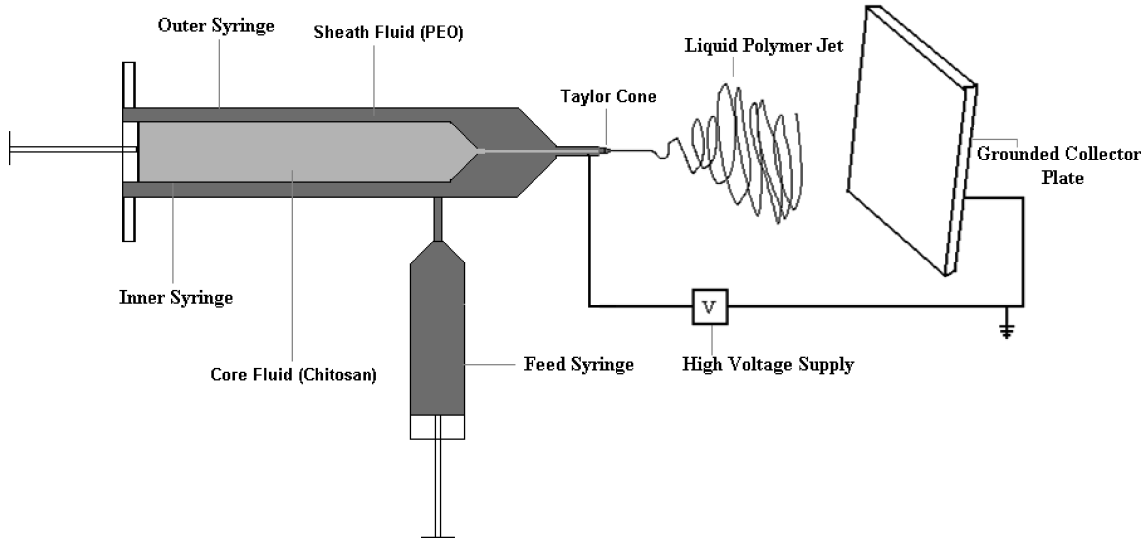


**Figure 1.** Diagram of experimental apparatus used for core-sheath electrospinning.

materials and here specifically demonstrate its use in forming chitosan nanofibers.

Chitosan ((1→4)-linked 2-amino-2-deoxy-$\beta$-D-glucan) is a linear polymer, the partially deacetylated form of chitin, obtained from crustaceans. It has been estimated that $10^{10}-10^{12}$ tons of chitin are biosynthesized each year.[19] Its biocompatible, biodegradable, and antimicrobial nature has resulted in significant research activity in fields such as drug delivery, tissue engineering scaffolds, and wound healing dressings.[20−24] The end products of degraded chitosan are natural metabolites, making it nontoxic and nonantigenic.[25] Despite these promising characteristics, the rigid D-glucosamine structures, high crystallinity, and intermolecular hydrogen bonds of chitosan, which restrict solubility in common organic solvents, and its tendency to form poly ions with anionic hydrocolloids that result in gel formation, have limited chitosan processability[23,26,27] and present a barrier to full utilization of this biomaterial.

Previously, chitosan nanofibers have been formed by electrospinning from strong acids,[28,29] from solutions of chitosan blended with synthetic polymer,[30−34] and by electrospinning chitin and then deacetylating the resultant fibers.[35]

Here we present an alternative approach (formation of a core-sheath structure and then removal of the sheath template) that may be more easily implemented to a wide variety of chitosan systems. In addition, we utilize IR spectroscopy, X-ray diffraction, mechanical property, and electrical conductivity measurements to characterize the resultant webs of the chitosan nanofibers.

## Experimental Section

**Materials.** Chitosan (82% deacetylated) was obtained from Sigma Aldrich having a viscosity average molecular wt of 148000 g/mol, as calculated from the intrinsic viscosity [$\eta$] using the Mark−Houwink equation, $[\eta] = KM\alpha$, where $K = 1.81 \times 10^{-3}$ mL/gm and $\alpha = 0.93$ from Maghami and Roberts.[36] The intrinsic viscosity [$\eta$] was measured in a mixture of 0.1 M acetic acid and 0.2 M sodium chloride at 25 °C. Polyethylene oxide ($M_w$ 900000 g/mol) was supplied by Scientific Polymers Products Inc. All samples were used without further purification. Chitosan solutions were prepared with varying concentrations (1−7 wt %) by dissolving chitosan in 90% acetic acid (EMD chemicals). For all the experiments concentration of the PEO solution (in water) was kept constant at 4 wt %.

**Sample Preparation.** *Electrospinning of Fibrous Mats.* Electrospinning of chitosan/PEO solutions was performed using a horizontal setup. A variable high voltage power supply (Glassman high voltage model #FC60R2 with positive polarity) generated a potential difference (15 kV) between the syringe and the collector plate. Two syringe pumps (New Era NE 500), kept perpendicular to each other, were used for pumping the polymer solutions at a feed rate of 50 $\mu$L/min with a tip-to-collector distance of 15 cm. Equal mass flow rate was maintained for core and sheath polymers. These parameters were chosen from an optimization of the PEO processing parameters, which is discussed in a previous work.[37] Because the processing window to produce homogeneous nanofibers is small, the core-sheath studies were focused around the optimal PEO processing conditions. Two concentric needles of gauge 16 and 22 G were used for sheath (PEO) and core (Chitosan) fluids, respectively. Both Chitosan and PEO solution were fed from 10 mL syringes. Figure 1 shows the core-sheath electrospinning setup. For electrical measurements, nanofibrous mats of thickness 30−150 $\mu$m were spun directly onto interdigitated electrodes, with the electrode placed on the collector plate. In addition, free-standing mats of ~1 mm thickness were also obtained by spinning on aluminum foil and then removing the mat from the foil. Mat thickness was measured with a micrometer for thicker samples and then extrapolated for thinner samples (assuming that the rate of deposition was constant throughout the spin).

*Removal of PEO Sheath.* The PEO layer was removed by carefully submerging the core-sheath fibrous mat adhered to the electrode substrate (via electrospinning) in deionized water for 24 h. The submersion and subsequent removal process (using tweezers) was on the order of a minute for each step. It is germane to note that when this process was rushed, the nanofibrous mat would be completely removed from the substrate surface.

*Film Fabrication.* Chitosan films were cast by placing a drop of 3 wt % in 90% acetic acid/water onto a glass slide (or a glass slide patterned with an interdigitated electrode), which spread and dried to a uniform film. Chitosan films were subjected to 0.5 h soaks in 2% sodium hydroxide immediately before swelling with water to neutralize any remaining acetic acid. For electrical measurements, free-standing films (first cast, and then peeled from the surface) were also measured by (1) fabrication of contacts with silver epoxy, (2) placing swollen films onto interdigitated electrodes, or (3) placing swollen films between parallel electrode plates.

**Characterization.** *Rheology.* The StressTech HR (ATS RheoSystems, Bordentown, NJ), a stress controlled rheometer, was used to obtain the zero-shear rate viscosity ($\eta_0$). For the initial studies, a 50 mm parallel plate was used to collect the viscosity data. The gap used for all

solutions was 0.300 mm at a temperature of 25 °C ± 0.1 °C. Additionally, to reach low shear rates with a low viscosity sample (less than 1000 cP), a custom-made, double-gap, concentric cylinder geometry was used. The outer radius of the bob measures 26.22 mm, with an inner radius of 21.60 mm. A volume of 2.83 $cm^3$ is required for accurate measurements. This fixture allowed for precise viscosity measurements at low concentrations of chitosan.

*Fourier Transform Infrared Spectroscopy.* Fourier transform infrared spectroscopy (FTIR) was performed (Nicolet Nexus 470) having 10 $\mu$m viewing area with single bounce attenuated reflectance device (OMNI Sampler with Ge crystal). FTIR of pure chitosan, pure PEO, and chitosan-PEO core-sheath nanofibers (before and after PEO washing) was performed.

*Scanning and Transmission Electron Microscopy.* To determine the surface morphology of nanofibers obtained from coaxial electrospinning, scanning electron microscopy (SEM) was performed using JEOL JSM-6400 FE with Energy Dispersive X-ray Spectroscopy (EDS) operating at 5 kV. Coaxial nanofibers samples were collected on aluminum foil and were sputter coated by a K-550X sputter coater with Au/Pd having thickness ~100 Å to reduce charging.

Transmission electron scanning (TEM) was performed using FEI/Philips EM 208S operating at 80 kV. The electrospun nanofibers were directly deposited on copper grids coated with a layer of Formvar and carbon film.

*Mechanical Properties.* Mechanical properties were tested using an Instron Model 5544 using the Bluehill version 1.00 software. Samples were prepared according to ASTM standard D4762-04. Each sample tested up to seven specimens with a gauge length of 3 cm and an average thickness of 0.12 mm. The testing rate was 5 mm/min. Samples were tested within 24 h of fabrication. The volume fraction of voids in the mat was taken into consideration for the mechanical property calculations. The void measurement and calculation is described below.

The volume of voids in the random fibrous mats was calculated from SEM images using Image J analyzer. Different layers of nanofibers were made distinct using grayscale. The area (proportional to volume) of nanofibers present in one plane was then calculated, and therefore, the void fraction was calculated in a single layer. This procedure was repeated four times for each sample for statistical purposes.

*Electrical Properties.* Electrical measurements utilized both planar interdigitated electrodes on glass and sandwich-like electrode configurations to measure the highly porous mats of nanofibers, as well as cast films for comparison. Interdigitated electrodes consist of two planar "combs" each containing a contact pad and 25 fingers or digits, where the digits from each comb alternate, akin to two hands with the fingers interweaved. Samples in vacuum (~$10^{-7}$ torr), at ambient conditions, and after 1 h soaks in deionized water, were measured. Each interdigitated electrode was measured before mat or film deposition, with this measured conductance, ~$1 \times 10^{-14}$ S in vacuum or ~$1 \times 10^{-14}$−$1 \times 10^{-13}$ S at ambient, setting the measurement limit of our system. The leakage current of the parallel plate configuration was ~$10^{-14}$ S/cm in vacuum. Interdigitated electrodes were fabricated from conventional lift-off UV-lithography.[37] Digit spacing could be varied from 10 to 100 $\mu$m. A sensitive Keithley (6430 subfemtoamp) source-measurement unit was used to obtain current−voltage characteristics, which were analyzed to determine electrical conductance. The measured porosity of the mats was taken into account when calculating mat conductivity. All errors reported are standard deviations.

It is well-known that interdigitated electrodes generate significant fringe fields that penetrate above and below the electrode plane, with the depth of penetration proportional to the electrode finger spacing.[38] Based on the calculated field patterns of our interdigitated electrode configuration,[39] values for estimated conductivity were calculated. In particular, assuming a large number of electrode finger pairs and negligible finger height compared to other electrode and sample dimensions, an estimate of the electric field versus depth was obtained. As a final check of this technique, very thick films and mats were measured by placing them between metal parallel plates (2.5 cm square), spaced by insulating glass of either 0.25 or 0.5 mm thickness.

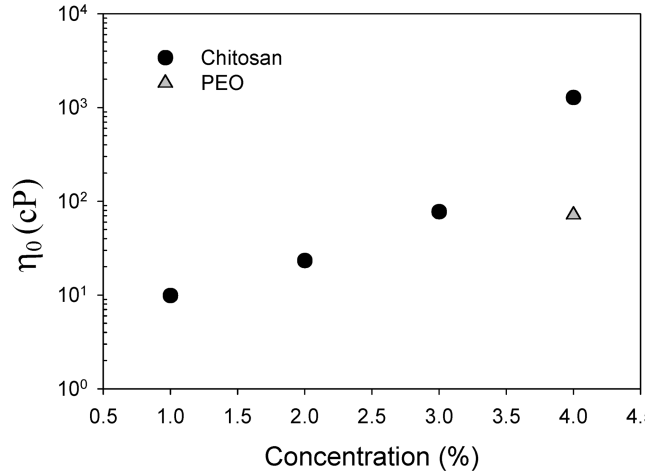


**Figure 2.** The concentration dependence of the zero shear rate viscosity ($\eta_0$; in centipoise) for chitosan and PEO. The black circles indicate $\eta_0$ for varying concentrations of chitosan (1−4 wt %) and the gray triangle indicates $\eta_0$ for 4 wt % PEO.

In addition to DC measurements, for some samples, AC measurements at 26 different frequencies between 50 Hz and 20 kHz were taken with an Andeen-Hagerling 2700A sensitive capacitance bridge, measuring parallel resistance. The AC values were compared to the form $\sigma(\omega) = \sigma_{DC}[1 + (\omega/\omega_p)^n]$ to obtain $\sigma_{DC}$ estimates.[40,41] Here $\sigma$ is conductivity, $\omega = 2\pi f$, where $f$ is the linear frequency, and $n$ is an exponent limited to $0 < n < 1$. This model assumes ionic conductivity due to thermally activated hopping, with a temperature dependent hopping frequency of $\omega_p$. A previous conductivity study of chitosan (doped with ammonium triflate salt) found $(\omega_p/2\pi)$ ~10 kHz at room temperature.[42] Thus, a flat, lower frequency range of our data was used to estimate the DC conductivity.

## Results and Discussion

**Processing Considerations.** Rheological experiments were performed on the chitosan solutions to determine useful concentrations for coaxial spinning. Zero shear rate viscosity ($\eta_0$) versus concentration is plotted in Figure 2. Because previous work in our laboratory[37] has shown that 4 wt % PEO (in water) can be electrospun into defect-free nanofibers, the objective of rheological experiments was to find the chitosan concentration with a similar zero shear rate viscosity.[16,43] As seen in Figure 2, the $\eta_0$ of 3 wt % chitosan (77 cP) and 4 wt % PEO (72 cP) are nearly equivalent. Because the viscosities of these two solutions are similar, the amount of shear stress generated at the tip of the capillary in 4 wt % PEO and 3 wt % chitosan are closely matched. In fact, coaxial nanofibers were successfully electrospun only with this set of concentrations (3 wt % chitosan/4 wt % PEO), with comparable values of $\eta_0$. Other concentrations of chitosan resulted in spraying of the solution rather than jetting.

The transmission electron micrographs in Figure 3 show the formation of core-sheath nanofibers with good contrast between the core and sheath components. As stated previously, different concentrations of chitosan were evaluated (between 1−7 wt %) but the core-sheath morphology was observed with only 3 wt % chitosan solution (as core) together with 4 wt % PEO solution (as sheath). At other concentrations of chitosan, no stable jet formation was obtained. It can be seen that the diameter of the sheath nanofibers obtained is around 250 nm and the diameter of the core nanofiber is around 100 nm.

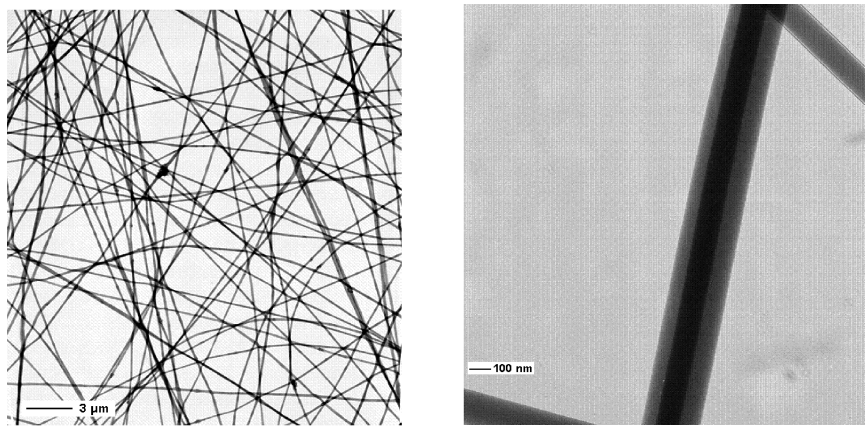


**Figure 3.** TEM images (a) low magnification and (b) high magnification of coaxially electrospun chitosan (3 wt %)−PEO (4 wt %) core-sheath fibers before washing the PEO layer.

**Table 1.** Mechanical Property Comparison of Pure PEO Nanofibers and Chitosan-PEO Core-Sheath Nanofibers before PEO Washing Step

| sample | tensile strength (MPa) | modulus (MPa) |
|---|---|---|
| pure PEO | $10.0 \pm 0.2$ | $12.3 \pm 1.5$ |
| chitosan-PEO | $4.0 \pm 0.3$ | $147 \pm 7$ |

**Characterization of the Core-Sheath Structures.** Tensile tests were performed to evaluate the changes in the mechanical properties of nanofibrous mats due to the formation of the core-sheath structure. Void space within the fibrous mats was taken into account in analysis of the mechanical measurements, using the average void volume fraction (obtained from SEM images using Image J analyzer) of 84%. Compared with our previous findings for pure PEO,[37] it is evident that the introduction of chitosan as the core material resulted in a slight decrease in the tensile strength, while the modulus showed a significant increase (as shown in Table 1). Obviously, the introduction of chitosan in the core significantly improved the modulus of the nanofibrous mat (due to the increased stiffness of chitosan compared to PEO), but made the overall structure slightly more brittle. We hypothesize that the reduction in mat strength is a result of weaker interface between the chitosan core and the PEO sheath. In effect, this would be similar to decreasing the adhesion at fiber−fiber contacts (which would also greatly compromise the strength of the fibrous mat at higher loads).

**Removal of the Sheath.** After electrospinning of the core-sheath structure, the PEO sheath layer was removed by soaking in deionized water (as discussed in the Experimental Section, "Removal of the PEO Sheath"). Scanning electron micrographs (as shown in Figure 4) were taken before and after the mats were washed with water. The images show that the structure and integrity of nanofibers is maintained after washing. (The morphology of the chitosan fibers after sheath removal will be discussed in the next section.) Wide angle X-ray diffraction data of mats before and after water soaking is shown in Figure 5. As can be seen in Figure 5a, the unwashed PEO-chitosan mat (sample i) exhibits well-defined peaks at 19.9 and 24.0° $2\theta$, indicative of PEO crystallinity. The washed mat (sample ii), however, shows only two weak broad humps between 10 and 30° $2\theta$, indicative of the amorphous chitosan.[44] Figure 5b shows the intensity as a function of $2\theta$ for the washed mat (sample ii) compared to a pure chitosan film (sample iii). As can be seen, the weak humps are present for both samples, but appear slightly more intense for the chitosan film (which may indicate a higher degree of amorphous orientation), but in both cases, no intense crystalline peaks are observed. These results strongly support the hypothesis that the PEO is removed from the electrospun mat during the water treatment (washing).

Fourier transform infrared spectroscopy results also confirmed removal of the majority of PEO after water soaking. As shown in Figure 6, FTIR of mats before soaking confirmed peaks corresponding to chitosan and PEO in the core-sheath assembly. After washing, peaks corresponding to PEO were subdued (specifically the sharp peak at 2885 $cm^{-1}$ attributed to the $CH_2$ stretching). The broad feature between 3500−3100 $cm^{-1}$ attributed to intermolecular hydrogen bonding between chitosan molecules and NH and OH···O stretching was also smaller in the washed sample. Based on the relative absorbance of the broad chitosan hump and the PEO peak at 2885 $cm^{-1}$, we hypothesize that some PEO still remains in the interstitial fiber spaces which is unable to dissolve during the deionized water washing.

As discussed in detail below, the presence of the sheath was also confirmed by electrical measurements that showed no electrical conductivity for unwashed mats, where the conductive chitosan was fully covered by the insulating PEO layer, with an increase in conductivity (to match that of pure chitosan films) after the washing procedure. Therefore, microscopy, X-ray, FTIR, and conductivity data clearly indicate the removal of the PEO sheath layer in the nanofibrous mat structure.

**Properties of the Resultant Chitosan Fibers.** As observed in Figure 4, the morphology of the after-washed fibers is altered. The after-washed fibers appear to be flatter and more ribbon-like (rather than cylindrical) than the original core-sheath structure. We attribute this effect to the well-known swelling of chitosan in water and subsequent collapse as a result of the solvation and drying. In this work, no effort was made to slow the drying process; however, controlled drying or drying away from a surface might result in a more cylindrical resultant fiber. As a result of this process, the volume fraction of voids decreased from 84% for the unwashed sample to 70% in the washed sample. This may have negative implications for use as tissue engineering scaffolds, however, 70% porosity is a great improvement compared to a solid chitosan film. In addition, we are in the process of optimizing the process to improve overall structure (and, therefore, porosity).

Unfortunately, the washed mats were too fragile for completion of mechanical measurements, which might be of particular interest because, as discussed above, the solution used for

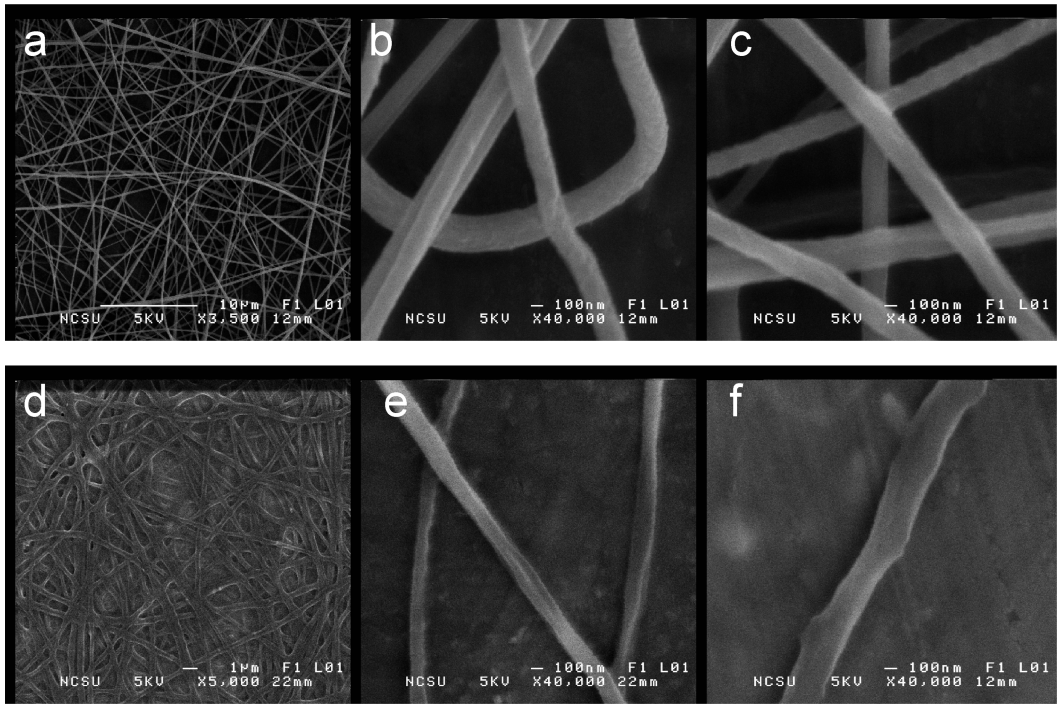


**Figure 4.** SEM images of electrospun chitosan-PEO core-sheath nanofibers. (a−c) Samples before $H_2O$ rinse and (d−f) samples after $H_2O$ rinse.

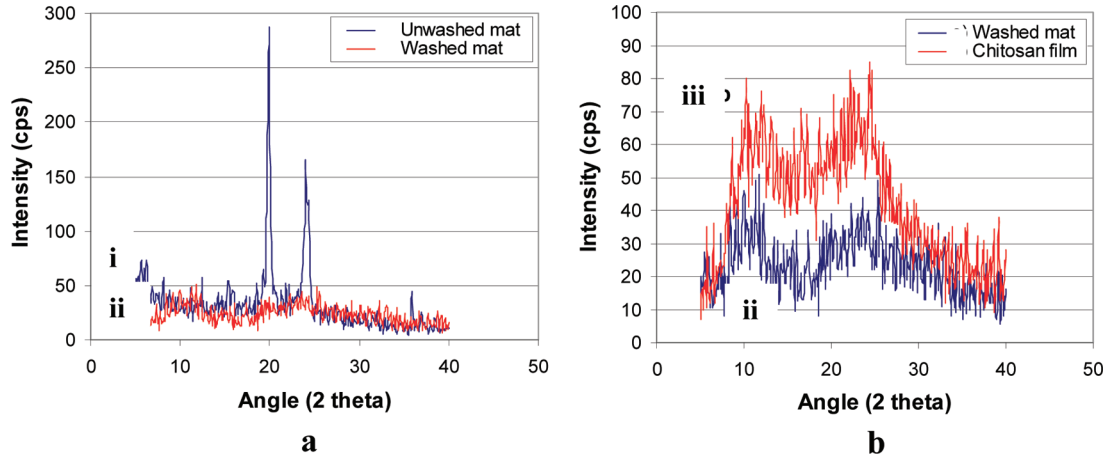


**Figure 5.** Wide-angle X-ray diffraction data for (a) the unwashed and washed electrospun mat and (b) the washed electrospun mat and a pure chitosan film.

electrospinning was below the critical entanglement threshold and, thus, could have a negative impact in the mechanical properties of the resultant fibers. In addition, as a result of the wash we expect the fiber-fiber contacts to be poorly bonded, thereby making the mats extremely fragile (because the fibrous mat is not confined during the wash step). The bond strength of the fiber−fiber contacts is extremely important (as discussed above for the mechanical properties of the PEO-chitosan samples).

We undertook electrical measurements to determine if chitosan retained an expected level of conductivity in the final fibrous mat. This would indicate the absence of blending with PEO, a similar crystallinity in nanofibers as drop-cast chitosan films, and a similar ability to swell in aqueous conditions. Natural biopolymers possess innate conductivity, usually due to ionic motion, with a strong dependence on water concentration.[45] Likewise, chitosan is a solid electrolyte that conducts ions when hydrated.[46]

Wan et al.[47] determined that dry chitosan films measured at ambient conditions (with molecular weights $3 \times 10^5$−$8 \times 10^5$ g/mol at 70−95% deacetylation) have conductivity in the range $1 \times 10^{-11}$−$1 \times 10^{-9}$ S/cm. This value rises to $1 \times 10^{-5}$−$1 \times 10^{-4}$ S/cm after exposure to water for 1 h or more. These authors proposed a mechanism whereby water protonates amine groups in the backbone forming mobile hydroxyl ions ($H_2O^+ \ NH_2 \rightarrow NH_3^+ + OH^-$).[47] In Wan's work, the lowest molecular weight chitosan ($3 \times 10^5$ g/mol) measured showed the smallest gains in conductivity with $\sigma_{max} = 1 \times 10^{-5}$ S/cm after water exposure. Furthermore, chitosan pellets with $M_W = 1.7 \times 10^4$ g/mol, 85% deacetylation, showed limited conductivity increases (from $10^{-9}$ to $10^{-7}$ S/cm) when increasing the relative humidity from 40 to 70% (7−15% water content in the pellet).[48] In a series of papers, Wan et al. concluded that crystallinity and the related ability of chitosan film to swell were the factors that limited the maximum hydrated conductivity.[49−51]

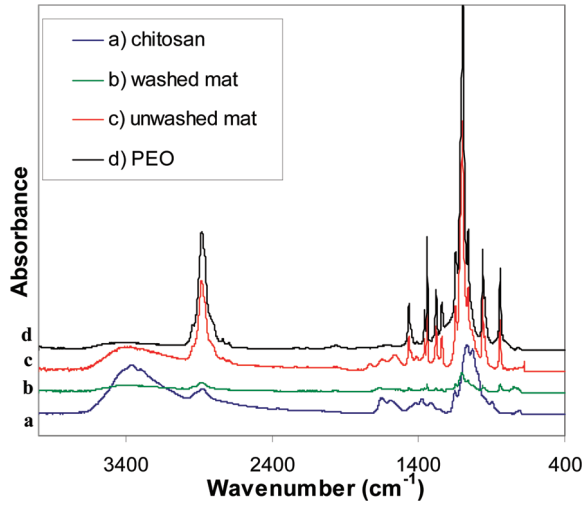


**Figure 6.** FTIR spectra of (a) chitosan, (b) electrospun PEO-chitosan nanofibers (after washing), (c) electrospun PEO-chitosan nanofibers (before washing), and (d) PEO.

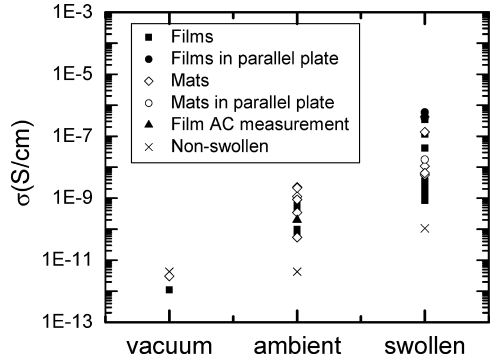


**Figure 7.** Conductivity vs sample condition for films and mats of chitosan. Mats, films, and an example of a mat that had very little swelling are shown. DC measurements (mats and films) took place on interdigitated or parallel plate electrodes and films were also subjected to AC measurements. Overall, for the 4 films and 8 mats measured at ambient, $\sigma$_film $= 3 \times 10^{-10} \pm 2.5 \times 10^{-10}$ S/cm and $\sigma$_mat $= 8.5 \times 10^{-10} \pm 9.3 \times 10^{-10}$ S/cm. Removing the two mat samples that exhibited no increase at ambient (no swelling) yields, $\sigma$_mat $= 1.2 \times 10^{-9} \pm 9 \times 10^{-10}$ S/cm. For the 12 films and 6 mats measured after exposure to water, $\sigma$_film $= 1.8 \times 10^{-7} \pm 2.4 \times 10^{-7}$ S/cm and $\sigma$_mat $= 1.2 \times 10^{-7} \pm 2.2 \times 10^{-7}$ S/cm. The large standard deviations represent difficulties in forcing some samples to swell. Utilizing the most reproducible sample preparations methods for swollen films (preswollen films placed on electrodes) and mats (free-standing PEO-chitosan mats placed on electrodes and then soaked to remove the PEO) we find $\sigma$_film increased from $1.2 \times 10^{-9} \pm 0.8 \times 10^{-9}$ S/cm to $8.1 \times 10^{-8} \pm 7.1 \times 10^{-8}$ S/cm, whereas $\sigma$_mat changed from $2.3 \times 10^{-9} \pm 1.8 \times 10^{-9}$ S/cm to $1.5 \times 10^{-8} \pm 0.5 \times 10^{-8}$ S/cm upon soaking, for three samples of each type. Thus, no difference is observed in chitosan conductivity as a function of morphology (fibrous mat versus homogeneous film) at ambient or swollen conditions.

As discussed above, mats of PEO-chitosan nanofibers (with one exception, perhaps due to incomplete coating with PEO) showed no conductance, that is, a current−voltage characteristic indistinguishable from the uncoated electrode. This result is consistent with the core-sheath picture where the highly insulating PEO completely encapulsates the chitosan core.

Figure 7 summarizes electrical experiments with chitosan mats and films. After washing with deionized water for 24 h to remove the PEO sheath, the chitosan mats were measured under vacuum and displayed an estimated conductivity ($\sigma$) of $\sim 10^{-12}$ S/cm. The same range of values was observed for drop-cast films and is consistent with previous reports.[52] Measuring samples under ambient conditions resulted in an increase of conductivity to $10^{-11}-10^{-9}$ S/cm, again with mats and films showing similar values. Two mats, which had been electrospun directly onto electrodes, showed artificially low values at ambient conditions and did not increase in conductivity from vacuum to ambient. These same mats also displayed a very small increase in conductivity when swollen with water. We believe this is due to strong adhesion of the mat to the electrode and substrate, which prevents swelling. An example of these results is included with a nonswollen designation in Figure 7. Overall, measurements for films and mats are consistent with the values of $1 \times 10^{-10}-1 \times 10^{-9}$ S/cm reported by several workers for dry, unmodified films at ambient conditions.[42,47,48,53] AC measurements confirmed these DC values.

Upon soaking samples in water, a range of conductivities, consistent with differences in observed swelling, were obtained. Electrical conductivity for wet films ranged from $10^{-9}$ S/cm (consistent with ambient conditions) to $\sim 10^{-7}$ S/cm, which is lower than the maximum conductivity reported by Wan et al.[47] for slightly higher molecular weight chitosan with a similar degree of deacetylation and consistent with Suzuki's results for chitosan pellets of similar molecular weight. We note that without soaking in sodium hydroxide to neutralize the acetic acid, larger values were occasionally obtained, presumably due to ions associated with the acetic acid.

Electrode polarization can occur in ion-conducting systems, where ions build up at electrode surfaces and decrease the effective electric field, resulting in artificially low conductivity values which depend on the electrode spacing. To check for this effect, we altered the electrode spacing from 10 to 100 $\mu$m and found that the average $\sigma$ increased by about an order of magnitude to $\sim 5 \times 10^{-7}$ S/cm. Utilizing parallel-plate configurations with electrode spacing of 0.25 or 0.5 mm, yielded $\sim 4 \times 10^{-7}$ S/cm (indistinguishable with our error), indicating that $\sim 5 \times 10^{-7}$ S/cm is the maximum conductivity in this system. AC measurements of swollen films confirmed this value, however, unlike the ambient measurement, $\sigma$ did decrease with decreasing frequency, even at low $\omega$, which may be an indication that some level of electrode polarization is present.

Swollen mats showed a similar range of conductivities to films, ranging from $5 \times 10^{-9}$ to $1 \times 10^{-7}$ S/cm. In particular, measurements of mats in the parallel-plate configuration showed $\sim 10^{-8}$ S/cm. In general, swelling of mats and films with water showed only moderate gains in conductivity. This is likely due to the particular properties (molecular weight and, perhaps, degree of deacetylation) of our chitosan, as this effect is seen in both films and mats, whereas our values for ambient conditions (which are less sensitive to the ability to swell) match well with the literature. Comparing the most reproducible data from films (preswollen films placed on electrodes) and mats (free-standing PEO-chitosan mats placed on electrodes and then soaked to remove the PEO), we find no difference in chitosan conductivity when swollen, despite different sample morphologies (see caption of Figure 7). Thus, electrical measurements support the core-sheath interpretation where the PEO can be completely removed and only chitosan fibers remain. Furthermore, our data shows no evidence of changes in crystallinity or swelling ability in comparing drop-cast films and electrospun fibers. However, repeating these experiments with a chitosan that displays more dramatic increases in conductivity upon hydration would further delineate any effect due to morphology.

## Conclusions

In the present work, we have demonstrated that chitosan fibers can be electrospun in a core-sheath configuration with a readily spinnable polymer (such as PEO) serving as a template sheath for the chitosan core. SEM, TEM, and electrical conductivity investigations confirm core sheath morphology of nanofibers. Tensile tests show that the addition of chitosan in the core negatively affected the tensile strength of the fibrous mats as compared to the pure PEO nanofibrous mats, which we believe is due to the relatively weak interface between the core and the sheath layers (similar to what is expected with poor fiber−fiber adhesion). Fourier transform infrared spectroscopy, X-ray diffraction, electron microscopy, and electrical measurements show that the PEO (outer layer) is removed by washing the core-sheath nanofibers in a water bath and that the resultant fibers are pure chitosan. Electrical measurements of chitosan films and mats of chitosan nanofibers were consistent, indicating that chitosan does not significantly change its crystallinity or other properties as a result of electrospinning. Finally, we note that the approach of templating by coaxial electrospinning is a useful and straightforward alternative technique for forming nanofibers of materials that are difficult to electrospin.

In more recent studies, we have reversed the materials in the core and sheath to produce bicomponent fibers with chitosan in the outer layer (which eliminates the washing step). These results will be reported in a follow-up publication. The potential for such nanofibers could be significant in biomedical fields involving wound care and tissue engineering.

**Acknowledgment.** We gratefully acknowledge Dr. Michael Dykstra and Abbey Wood for their efforts in performing TEM. We also thank Dr. Dale Batchelor for helping us with SEM.

## References and Notes

(1) Formhals,A. *U.S. Patent 1,975,504*, 1934.
(2) Reneker, D. H.; Chun, I. *Nanotechnology* **1996**, *7*, 216–223.
(3) Kenawy, E. R.; Bowlin, G. L.; Mansfield, K.; Layman, J.; Simpson, D. G.; Sanders, E. H.; Wnek, G. E. *J. Controlled Release* **2002**, *81*, 57–64.
(4) Li, D.; Wang, Y.; Xia, Y. *Nano. Lett.* **2003**, *3*, 1167–1171.
(5) Theron, A.; Zussman, E.; Yarin, A. L. *Nanotechnology* **2001**, *12*, 384–390.
(6) Huang, Z. M.; Zhang, Y. Z.; Kotaki, M.; Ramakrishna, S. *Compos. Sci. Technol.* **2003**, *63*, 2223–2253.
(7) Reznik, S. N.; Yarin, A. L.; Theron, A.; Zussman, E. *J. Fluid Mech.* **2004**, *516*, 349–377.
(8) Shenoy, S. L.; Bates, W. D.; Frisch, H. L.; Wnek, G. E. *Polymer* **2005**, *46*, 3372–3384.
(9) Jang, J.; Lim, B.; Lee, J.; Hyeon, T. *Chem Commun.* **2001**, 83–84.
(10) Morales, A. M.; Leiber, C. M. *Science* **1998**, *279*, 208–211.
(11) Bognitzki, M.; Hou, H.; Ishaque, M.; Frese, T.; Hellwig, M.; Schwarte, C.; Schaper, A.; Wendorff, J. H.; Greiner, W. *Adv. Mater.* **2000**, *12*, 637–640.
(12) Gupta, P.; Wilkes, G. L. *Polymer* **2003**, *44*, 6353–6359.
(13) Ojha, S. S.; Stevens, D. R.; Stano, K. L.; Hoffman, T. J.; Clarke, L. I.; Gorga, R. E. *Macromolecules* **2008**, *41*, 2509–2513.
(14) Reznik, S.; Yarin, A. L.; Zussman, E.; Berkovici, L. *Phys. Fluids* **2006**, *18*, 062101–062114.
(15) Dror, Y.; Salalha, W.; Avrahami, R.; Zussman, E.; Yarin, A. L.; Dersch, R.; Greiner, A.; Wendorff, J. H. *Small* **2007**, *3*, 1064–1073.
(16) Sun, Z.; Zussman, E.; Yarin, A.; Wendorff, J. H.; Greiner, A. *Adv. Mater.* **2003**, *15*, 1929–1932.
(17) Yu, J. H.; Fridrikh, S. V.; Rutledge, G. C. *Adv. Mater.* **2004**, *16*, 1562–1566.
(18) Du, J.; Hsieh, Y. L. *Cellulose* **2007**, *14*, 543–552.
(19) Percot, A.; Viton, C.; Domard, A. *Biomacromolecules* **2003**, *4*, 12–18.
(20) Suh, J. K.; Matthew, H. W. T. *Biomaterials* **2000**, *21*, 2589–2598.
(21) Borchard, G. *Adv. Drug Delivery Rev.* **2001**, *52*, 145–150.
(22) Tomihata, K.; Ikada, Y. *Biomaterials* **1997**, *18*, 567–575.
(23) De Vrieze, S.; Westbroek, P.; Van Camp, T.; Van Langenhove, L. *J. Mater. Sci.* **2007**, *42*, 8029–8034.
(24) Matsuda, A.; Kagata, G.; Kino, R.; Tanaka, J. *J. Nanosci. Nanotechnol.* **2007**, *7*, 852–855.
(25) Lee, W. F.; Chen, Y. J. *J. Appl. Polym. Sci.* **2001**, *82*, 2487–2496.
(26) Li, L.; Hsieh, Y. L. *Carbohydr. Res.* **2006**, *341*, 374–381.
(27) Amaike, M.; Senoo, Y.; Yaamoto, H. *Macromol. Rapid Commun.* **1998**, *19*, 287–289.
(28) Schiffman, J. D.; Schauer, C. L. *Biomacromolecules* **2007**, *8*, 2665–2667.
(29) Zhou, Y. S.; Yang, D. Z.; Nie, J. *Plast., Rubber Compos.* **2007**, *36*, 254–258.
(30) Bhattarai, N.; Edmondson, D.; Omid, V.; Matsen, F. A.; Zhang, M. *Biomaterials* **2005**, *26*, 6176–6184.
(31) Duan, B.; Dong, C.; Yuan, X.; Yao, K. *J. Biomater. Sci., Polym. Ed.* **2004**, *15*, 797–811.
(32) Jia, Y. T.; Gong, J.; Gu, X. H.; Kim, H. Y.; Dong, J.; Shen, X. Y. *Carbohydr. Polym.* **2007**, *67*, 403–409.
(33) Ohkawa, K.; Cha, D. I.; Kim, H.; Nishida, A.; Yamamoto, H. *Macromol. Rapid Commun.* **2004**, *25*, 1600–1605.
(34) Chen, C. Y.; Wang, J. W.; Hon, M. S. *Macromol. Mater. Eng.* **2006**, *291*, 123–127.
(35) Min, B. M.; Lee, S. W.; Lim, J. N.; You, Y.; Lee, T. S.; Kang, P. H.; Park, W. H. *Polymer* **2004**, *45*, 7137–7149.
(36) Maghami, G. G.; Roberts, G. A. F. *Makromol. Chem.* **1988**, *189*, 195–200.
(37) McCullen, S. D.; Stevens, D. R.; Roberts, W. A.; Ojha, S. S.; Clarke, L. I.; Gorga, R. E. *Macromolecules* **2007**, *40*, 997–1003.
(38) Van Gerwen, P.; Laureyn, W.; Laureys, W.; Huyberechts, G.; Op De Beeck, M.; Baert, K.; Suls, J.; Sansen, W.; Jacobs, P.; Hermans, L.; Mertens, R. *Sens. Actuators* **1998**, *49B*, 73–80.
(39) den Otter, M. *Sens. Actuators* **2002**, *96A*, 140–144.
(40) Jonscher, A. K. *Nature* **1977**, *267*, 673–679.
(41) Almond, D. P.; West, A. R. *Solid State Ionics* **1983**, *9 &10*, 277–282.
(42) Khiar, A. S. A.; Puteh, R.; Arof, A. K. *Physica B* **2006**, *373*, 23–27.
(43) Li, D.; Xia, Y. *Nano. Lett.* **2004**, *4*, 933–938.
(44) Zivanovic, S.; Li, J.; Davidson, P. M.; Kit, K. *Biomacromolecules* **2007**, *8*, 1505–1510.
(45) Gu, W. Y.; Jutiz, M. A. *J. Biomed. Eng.* **2002**, *124*, 790.
(46) López-Chávez, E.; Martínez-Magadán, J. M.; Oviedo-Roa, R.; Guzmán, J.; Ramírez-Salgado, J.; Marín-Cruz, J. *Polymer* **2005**, *46*, 7519.
(47) Wan, Y.; Creber, K. A. M.; Peppley, B.; Bui, V. T. *Polymer* **2003**, *44*, 1057.
(48) Suzuki, K.; Saimoto, H.; Shigemasa, Y. *Carbohydr. Polym.* **1999**, *39*, 145–150.
(49) Wan, Y.; Creber, K. A. M.; Peppley, B.; Bui, V. T. *J. Appl. Polym. Sci.* **2003**, *89*, 306.
(50) Wan, Y.; Creber, K. A. M.; Peppley, B.; Bui, V. T. *Macromol. Chem. Phys.* **2003**, *204*, 850.
(51) Wan, Y.; Creber, K. A. M.; Peppley, B.; Bui, V. T. *J. Polym. Sci., Part B: Polym. Phys.* **2004**, *42*, 1379.
(52) Tkaczyk, S. W.; Swiatek, J.; Mucha, M. *IEEE Trans. Dielectr. Electr. Insul.* **2001**, *8*, 411–412.
(53) Osman, Z.; Ibrahim, Z. A.; Arof, A. K. *Carbohydr. Polym.* **2001**, *44*, 167–173.

BM800551Q